Tuning Photophysical and Electrochemical Properties of Cationic Iridium(III) Complex Salts with Imidazolyl Substituents by Proton and Anions

Qiang Zhao,[†] Shujuan Liu,[‡] Mei Shi,[†] Fuyou Li,*[,†] Hao Jing,[†] Tao Yi,[†] and Chunhui Huang*[,†]

Department of Chemistry and Laboratory of Advanced Materials, Fudan University, Shanghai, 200433, People's Republic of China, and Institute of Advanced Materials (IAM), Nanjing University of Posts and Telecommunications, 66 XinMoFan Road, Nanjing 210003, People's Republic of China

Received June 22, 2007

A series of cationic iridium(III) complex salts, **1**−**5**, were synthesized containing different phenanthroline derivatives. Their photophysical and electrochemical properties were investigated. The influences of anions and proton on the photophysical and electrochemical properties were also studied in detail. Upon addition of CF_3COOH, the emission wavelength was significantly red-shifted and the emission color changed from yellow to red. In addition, the addition of F^-, CH_3COO^-, and $H_2PO_4^-$ can also cause significant variations in UV−vis absorption and emission spectra. Upon addition of F^-, CH_3COO^-, and $H_2PO_4^-$, the solution colors of **1**−**3** changed from yellow-green to brown and the emission of **1**−**3** was quenched completely, which can be observed by the naked eye.

Introduction

Phosphorescent heavy-metal complexes have been explored for a multitude of photonic applications including organic light-emitting diodes,[1] photovoltaic cells,[2] biological labeling reagents,[3] and hydrogen production via photoreduction of water.[4] Recently, phosphorescent heavy-metal complexes have also attracted considerable interest as sensors,[5] because of their significant Stokes shifts for easy separation of excitation and emission and relatively long lifetimes compared with purely organic luminophores.[6] Many phosphorescent heavy-metal complexes, such as platinum(II), rhenium(I), and ruthenium(II) complexes, have been explored as chemosensors for anions,[7] oxygen concentration,[8] and metal ions.[5c] However, as the best phosphorescent dyes,[9] the applications of iridium(III) complexes in chemosensors were mainly limited to recognizing oxygen[10] and the Hg^{2+} cation.[11]

On the other hand, anion recognition and sensing have been of most interest in recent years because of their important roles in biological processes and environmental assays.[12] Various types of pure organic dyes have been used as receptors for anionic species.[12,13] Up to now, only one example of iridium(III) complex salts has been reported to recognize chloride anions with low sensitivity ($Ksv^{-1} = 34$ mmol L^{-1}).[14]

In our previous report, the imidazolyl group of imidazo[4,5-*f*][1,10]phenanthroline can interact with a proton, and the NH group can also be deprotonated by addition of a strong alkali.[15] Sensitivity to proton and alkali might be expected for iridium(III) complexes incorporating an imidazo[4,5-*f*][1,10]-phenanthroline unit. Herein, three cationic iridium(III) complex salts $[Ir(ppy)_2(N\wedge N)]^+PF_6^-$ (**1**−**3**) (see Chart 1) based on different phenanthroline derivatives (N^N ligands) were synthesized, and the tuning of the photophysical and electrochemical

* To whom correspondence should be addressed. Fax: 86-21-55664621. Tel: 86-21-55664185. E-mail: fyli@fudan.edu.cn (F.Y.L.); chhuang@pku.edu.cn (C.H.H.).

[†] Fudan University.

[‡] Nanjing University of Posts and Telecommunications.

(1) (a) Tsuboyama, A.; Iwawaki, H.; Fururori, M.; Mukaide, T.; Kamatani, J.; Igawa, S.; Moriyama, T.; Miura, S.; Takiguchi, T.; Okada, S.; Hoshino, M.; Ueno, K. *J. Am. Chem. Soc.* **2003**, *125*, 12971−12979. (b) Adachi, C.; Baldo, M. A.; Thompson, M. E.; Forrest, S. R. *J. Appl. Phys.* **2001**, *90*, 5048−5051.

(2) (a) Wong, H. L.; Lam, L. S. M.; Cheng, K. W.; Man, K. Y. K.; Chan, W. K.; Kwong, C. Y.; Djurišić, A. B. *Appl. Phys. Lett.* **2004**, *84*, 2557−2559. (b) Hara, K.; Nishikawa, T.; Kurashige, M.; Kawauchi, H.; Kashima, T.; Sayama, K.; Aika, K.; Arakawa, H. *Solar Energy Mater. Solar Cells* **2005**, *85*, 21−30.

(3) Lo, K. K. W.; Ng, D. C. M.; Chung, C. K. *Organometallics* **2001**, *20*, 4999−5001.

(4) (a) Goldsmith, J. I.; Hudson, W. R.; Lowry, M. S.; Anderson, T. H.; Bernhard, S. *J. Am. Chem. Soc.* **2005**, *127*, 7502−7510. (b) Kirch, M.; Lehn, J. M.; Sauvage, J. P. *Helv. Chim. Acta* **1979**, *62*, 1345−1384. (c) Krishnan, C. V.; Brunschwig, B. S.; Creutz, C.; Sutin, N. *J. Am. Chem. Soc.* **1985**, *107*, 2005−2015.

(5) (a) de Silva, A. P.; Gunaratne, H. Q. N.; Gunnlaugsson, T.; Huxley, A. J. M.; McCoy, C. P.; Rademacher, J. T.; Rice, T. E. *Chem. Rev.* **1997**, *97*, 1515−1566. (b) Demas, J. N.; DeGraff, B. A. *Coord. Chem. Rev.* **2001**, *211*, 317−351. (c) Tang, W. S.; Lu, X. X.; Wong, K. M. C.; Yam, V. W. W. *J. Mater. Chem.* **2005**, *15*, 2714−2720.

(6) Carraway, E. R.; Demas, J. N.; DeGraff, B. A.; Bacon, J. R. *Anal. Chem.* **1991**, *63*, 337−342.

(7) Lin, Z. H.; Zhao, Y. G.; Duan, C. Y.; Zhang, B. G.; Bai, Z. P. *Dalton Trans.* **2006**, 3678−3684.

(8) Brinas, R. P.; Troxler, T.; Hochstrasser, R. M.; Vinogradov, S. A. *J. Am. Chem. Soc.* **2005**, *127*, 11851−11862.

(9) (a) Neve, F.; Deda, M. L.; Crispini, A.; Bellusci, A.; Puntoriero, F.; Campagna, S. *Organometallics* **2004**, *23*, 5856−5863. (b) Liu, S. J.; Zhao, Q.; Chen, R. F.; Deng, Y.; Fan, Q. L.; Li, F. Y.; Wang, L. H.; Huang, C. H.; Huang, W. *Chem.−Eur. J.* **2006**, *12*, 4351−4361. (c) Didier, P.; Ortmans, L.; Kirsch-De Mesmaeker, A.; Watte, R. *Inorg. Chem.* **1993**, *32*, 5239−5245. (d) Zhao, Q.; Liu, S. J.; Shi, M.; Wang, C. M.; Yu, M. X.; Li, L.; Li, F. Y.; Yi, T.; Huang, C. H. *Inorg. Chem.* **2006**, *45*, 6152−6160.

(10) (a) Gao, R.; Ho, D. G.; Hernandez, B.; Selke, M.; Murphy, D.; Djurovich, P. I.; Thompson, M. E. *J. Am. Chem. Soc.* **2002**, *124*, 14828−14829. (b) Huynh, L.; Wang, Z.; Yang, J.; Stoeva, V.; Lough, A.; Manners, I.; Winnik, M. A. *Chem. Mater.* **2005**, *17*, 4765−4773. (c) Di Marco, G.; Lanza, M.; Mamo, A.; Stefio, I.; Di Pietro, C.; Romeo, G.; Campagna, S. *Anal. Chem.* **1998**, *70*, 5019−5023.

(11) Zhao, Q,; Cao, T.Y.; Li, F. Y,; Li, X.H.; Jing, H.; Yi, T.; Huang C. H. *Organometallics* **2007**, 26, 2077−2081.

(12) (a) Beer, P. D.; Gale, P. A. *Angew. Chem., Int. Ed.* **2001**, *40*, 486−516. (b) *Coord. Chem. Rev.* **2003**, *240*, issues 1 and 2 (Special Issues on anion receptors). (c) Martínez-Máñez, R.; Sancenón, F. *Chem. Rev.* **2003**, *103*, 4419−4476. (d) Suksai, C.; Tuntulani, T. *Chem. Soc. Rev.* **2003**, *32*, 192−202.

10.1021/om700623j CCC: $37.00
Publication on Web 10/24/2007

Chart 1. Chemical Structures of the Complex Salts 1−5

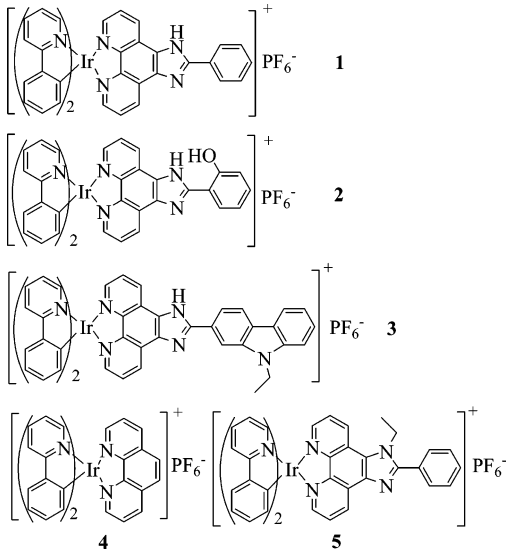

properties of **1**−**3** by anions and proton was investigated. For comparison, two other cationic iridium(III) complex salts, $[Ir(ppy)_2(L2)]^+PF_6^-$ (**4**) and $[Ir(ppy)_2(L3)]^+PF_6^-$ (**5**), without the N−H group were also studied.

Experimental Section

General Experiments. Commercially available chemical reagents were used without further purification. NMR spectra were taken on a Mercury Plus 400 MHz NMR spectrometer. Elemental analyses were performed on a VarioEL III O-Element analyzer system. Mass spectra were obtained on a Shimadzu matrix-assisted laser desorption/ionization time-of-flight mass spectrometer (MALDI-TOF-MASS). UV−visible absorption spectra were recorded using a Shimadzu 3000 UV−vis−NIR spectrophotometer. Photoluminescence spectra were measured on an Edinburgh LFS920 fluorescence spectrophotometer. Luminescence quantum yields of the iridium complex salts in solution were measured with reference to quinine sulfate ($\Phi_F = 0.56$ in 1 mol L^{-1} sulfuric acid). The solutions were degassed by three freeze−pump−thaw cycles. Photoluminescent lifetime was recorded on a single photon counting spectrometer from Edinburgh Instruments (FLS920) with a hydrogen-filled pulse lamp as the excitation source. The data were analyzed by iterative convolution of the luminescence decay profile with the instrument response function using the software package provided by Edinburgh Instruments.

Materials. $IrCl_3 \cdot 3H_2O$, phenanthroline, benzaldehyde, and 2-hydroxybenzaldehyde were industrial products and used without further purification. 2-Phenylpyridine and *N*-ethyl-3-carbazolecarboxaldehyde were obtained from Acros and used without further purification.

Synthesis of the Phenanthroline Derivatives. The phenanthroline derivatives were synthesized according to a previous report.[16]

Synthesis of the Iridium(III) Complex Salts. All iridium(III) complex salts $[Ir(ppy)_2(N\wedge N)]^+PF_6^-$ were prepared by the same procedure. Herein, only the synthesis of complex salt $[Ir(ppy)_2(phen)]^+PF_6^-$ (**1**) is described in detail.

Complex Salt 1. The cyclometalated iridium(III) chlorobridged dimer $[Ir(ppy)_2Cl]_2$ was prepared according to literature methods.[17] A solution of $[Ir(ppy)_2Cl]_2$ (0.079 mmol) and 2-phenylimidazo-[4,5-*f*][1,10]phenanthroline (0.158 mmol) in CH_2Cl_2−MeOH (30 mL, 2:1 v/v) was heated to reflux. After 4 h, the yellow solution was cooled to room temperature, and then a 10-fold excess of potassium hexafluorophosphate was added. The suspension was stirred for 2 h and then was filtered to remove insoluble inorganic salts. The solution was evaporated to dryness under reduced pressure. The crude product was applied to a silica gel column and eluted with CH_2Cl_2−acetone (15:1) to afford a yellow solid in 63% yield. ^{1}H NMR (400 MHz, d_6-DMSO), δ(ppm): 9.15 (d, 2H, J = 8.0), 8.26 (t, 4H, J = 8.0), 8.15 (d, 2H, J = 4.0), 8.03−8.07 (m, 2H), 7.95 (d, 2H, J = 7.6), 7.86 (t, 2H, J = 7.6), 7.63 (t, 2H, J = 7.2), 7.56 (t, 1H, J = 7.2), 7.51 (d, 2H, J = 5.6), 7.05 (d, 2H, J = 7.2), 6.92−6.99 (m, 4H), 6.30 (d, 2H, J = 7.2). ^{13}C NMR (100 MHz, d_6-DMSO), δ(ppm): 167.5, 153.4, 151.0, 149.8, 149.1, 144.8, 144.7, 139.3, 132.9, 131.9, 130.9, 129.9, 127.7, 127.2, 125.7, 124.5, 123.1, 120.6. Anal. Calcd for $IrC_{41}H_{28}N_6F_6P$: C, 52.28; H, 3.00; N, 8.92. Found: C, 52.42; H, 3.32; N, 8.67. MS(LDI-TOF): *m*/*e* 797.3 (M − PF_6).

Complex Salt 2. Yield: 57%. ^{1}H NMR (400 MHz, d_6-DMSO), δ(ppm): 9.25 (d, 2H), 8.16−8.26 (m, 6H), 8.06−8.09 (m, 2H), 7.95 (d, 2H), 7.86 (t, 2H), 7.51 (d, 2H), 7.43 (t, 1H), 7.03−7.13 (m, 4H), 6.93−6.99 (m, 4H), 6.29 (d, 2H). ^{13}C NMR (100 MHz, d_6-DMSO), δ(ppm): 167.5, 157.8, 153.1, 150.9, 149.8, 149.3, 144.9, 139.4, 138.6, 133.2, 132.8, 131.9, 130.9, 127.8, 127.6, 125.7, 124.5, 123.1, 120.6, 120.2, 118.0, 113.7, 56.7, 19.2. Anal. Calcd for $IrC_{41}H_{28}N_6F_6PO$: C, 51.41; H, 2.95; N, 8.77. Found: C, 51.21; H, 2.66; N, 8.43. MS(LDI-TOF): *m*/*e* 813.3 (M − PF_6).

Complex Salt 3. Yield: 55%. ^{1}H NMR (400 MHz, d_6-DMSO), δ(ppm): 9.21 (d, 2H, J = 8.4), 9.05 (s, 1H), 8.41 (d, 1H, J = 8.4), 8.27 (t, 3H, J = 6.8), 8.05−8.17 (m, 4H), 7.96 (d, 2H, J = 7.6), 7.87 (t, 3H, J = 8.4), 7.70 (d, 1H, J = 8.4), 7.53 (m, 3H), 7.30 (t, 1H, J = 7.6), 6.93−7.07 (m, 6H), 6.30 (d, 2H, J = 7.6), 4.50−4.55 (m, 2H), 1.37 (t, 3H, J = 7.2). ^{13}C NMR (100 MHz, d_6-DMSO), δ(ppm): 167.7, 154.7, 151.0, 149.5, 148.8, 144.6, 144.4, 141.3, 140.8, 139.2, 132.8, 131.9, 130.8, 127.3, 127.0, 125.6, 124.3, 123.2, 122.8, 121.0, 120.8, 120.6, 120.2, 119.5, 38.0, 14.4. Anal. Calcd for $IrC_{49}H_{35}N_7F_6P$: C, 55.57; H, 3.33; N, 9.26. Found: C, 55.76; H, 3.55; N, 9.40. MS(LDI-TOF): *m*/*e* 914.3 (M − PF_6).

Complex Salt 4. Yield: 65%. ^{1}H NMR (400 MHz, d_6-DMSO), δ(ppm): 8.91 (d, 2H, J = 8.0), 8.39 (s, 2H), 8.27 (d, 2H, J = 8.0), 8.20 (d, 2H, J = 5.2), 8.04−8.07 (m, 2H), 7.96 (d, 2H, J = 8.0), 7.88 (t, 2H, J = 7.6), 7.47 (d, 2H, J = 6.0), 7.07 (t, 2H, J = 7.2), 6.90−7.01 (m, 4H), 6.30 (d, 2H, J = 7.6). ^{13}C NMR (100 MHz, d_6-DMSO), δ(ppm): 167.5, 151.3, 150.5, 149.8, 146.7, 144.7, 139.5, 139.4, 131.9, 131.8, 130.9, 129.0, 127.8, 125.7, 124.5, 123.1, 120.6. Anal. Calcd for $IrC_{34}H_{24}N_4F_6P$: C, 49.45; H, 2.93; N, 6.78. Found: C, 49.23; H, 2.72; N, 6.45. MS(LDI-TOF): *m*/*e* 681.2 (M − PF_6).

Complex Salt 5. Yield: 50%. ^{1}H NMR (400 MHz, $CDCl_3$), δ(ppm): 9.30 (d, 1H, J = 8.4), 9.14 (d, 1H, J = 8.4), 8.24 (t, 2H, J = 4.8), 8.02−8.05 (m, 1H), 7.89−7.96 (m, 2H), 7.68−7.79 (m,

(13) For recent examples: (a) Bondy, C. R.; Gale, P. A.; Loeb, S. J. *J. Am. Chem. Soc.* **2004**, *126*, 5030−5031. (b) Chmielewski, M. J.; Charon, M.; Jurczak, J. *Org. Lett.* **2004**, *6*, 3501−3504. (c) Nielsen, K. A.; Jeppesen, J. O.; Levillain, E.; Becher, J. *Angew. Chem., Int. Ed.* **2003**, *42*, 187−191. (d) Wallace, K. J.; Belcher, W. J.; Syed, K. F.; Seed, J. W. *J. Am. Chem. Soc.* **2003**, *125*, 9699−9715. (e) Best, M. D.; Tobey, S. L.; Anslyn, E. V. *Coord. Chem. Rev.* **2003**, *240*, 3−15. (f) Choi, K.; Hamilton, A. D. *Coord. Chem. Rev.* **2003**, *240*, 101−110. (g) Mizuno, T.; Wei, W.-H.; Eller, L. R.; Sessler, J. L. *J. Am. Chem. Soc.* **2002**, *124*, 1134−1135. (h) Haj-Zaroubi, M.; Mitzel, N. W.; Schmidtchen, F. P. *Angew. Chem., Int. Ed.* **2002**, *41*, 104−107. (i) Liu, Z. Q.; Shi, M.; Li, F. Y.; Fang, Q.; Chen, Z. H.; Yi, T.; Huang, C. H. *Org. Lett.* **2005**, *7*, 5481−5484. (j) Zhou, Z. G.; Xiao, S. Z.; Xu, J.; Liu, Z. Q.; Shi, M.; Li, F. Y.; Yi, T.; Huang, C. H. *Org. Lett.* **2006**, *8*, 3911−3914. (k) Zhou, Z. G.; Yang, H.; Shi, M.; Xiao, S. Z.; Li, F. Y.; Yi, T.; Huang, C. H. *ChemPhysChem* **2007**, *8*, 1289−1292.

(14) Goodall, W.; Williams, J. A. G. *J. Chem. Soc., Dalton Trans.* **2000**, 2893−2896.

(15) Xiao, S. Z.; Tao Yi, T.; Zhou, Y. F.; Zhao, Q.; Li, F. Y.; Huang, C. H. *Tetrahedron* **2006**, *62*, 10072−10078.

(16) Han, M. J.; Gao, L. H.; Wang, K. Z. *New J. Chem.* **2006**, *30*, 208−214.

(17) Nonoyama, K. *Bull. Chem. Soc. Jpn.* **1974**, *47*, 467−468.

7H), 7.58−7.61 (m, 3H), 7.45 (d, 1H, $J = 5.6$), 7.34 (d, 1H, $J = 5.6$), 7.07−7.11 (m, 2H), 6.95−7.01 (m, 3H), 6.82 (t, 1H, $J = 7.2$), 6.39−6.42 (m, 2H), 4.75−4.88 (m, 2H), 1.65 (t, 3H, $J = 7.2$). ^{13}C NMR (100 MHz, d_6-DMSO), δ(ppm): 167.5, 155.6, 151.5, 150.9, 149.8, 149.7, 148.8, 145.1, 144.8, 144.7, 144.6, 139.4, 137.1, 132.9, 132.6, 131.9, 131.0, 130.9, 130.4, 130.1, 129.7, 128.2, 127.7, 126.8, 126.4, 125.7, 124.6, 124.5, 123.0, 122.9, 120.7, 29.7, 16.2. Anal. Calcd for $IrC_{43}H_{32}N_6F_6P$: C, 53.39; H, 3.34; N, 8.69. Found: C, 53.61; H, 3.15; N, 8.97. MS(LDI-TOF): *m/e* 825.3 (M − PF_6).

Theoretical Calculations. The calculations were performed using the Gaussian 03 suite of programs.[18] The starting geometry was from the single-crystal structure of complex salt **1**. DFT calculations (full geometry optimization) were carried out by B3LYP. The LANL2DZ basis set was used to treat the iridium atom, whereas the 3-21G* basis set was used to treat all other atoms. The contours of the HOMO and LUMO orbitals were plotted.

Electrochemical Measurements. Electrochemical measurements were carried out in a one-compartment cell under an N_2 atmosphere, equipped with a glassy-carbon working electrode, a platinum wire counter electrode, and an Ag/Ag^+ reference electrode with an Eco Chemie Autolab. Measurements of oxidation and reduction were undertaken in the anhydrous solution of CH_2Cl_2 and THF, respectively, containing the supported electrolyte of 0.10 mol L^{-1} tetrabutylammonium hexafluorophosphate ($Bu_4N^+ \cdot PF_6^-$). The scan rate was 50 mV s^{-1}.

X-ray Crystallography Analysis. The single crystal of the complex salt **1** was mounted on a glass fiber and transferred to a Bruker SMART CCD area detector. Crystallographic measurement was carried out using a Bruker SMART CCD diffractometer, σ scans, and graphite-monochromated Mo Kα radiation ($\lambda = 0.71073$ Å) at room temperature. The structure was solved by direct methods and refined by full-matrix least-squares on F^2 values using the program SHELXS-97.[19] All non-hydrogen atoms were refined anisotropically. Hydrogen atoms were calculated in ideal geometries. For the full-matrix least-squares refinements [$I > 2\sigma(I)$], the unweighted and weighted agreement factors of $R_1 = \sum(F_o - F_c)/\sum F_o$ and $wR_2 = [\sum w(F_o^2 - F_c^2)^2/\sum wF_o^4]^{1/2}$ were used. The crystal data and details of the structure determinations are summarized in Table 1. CCDC reference number for **1** is 628443.

Results and Discussion

Synthesis. The phenanthroline derivative ligands were synthesized according to previous reports.[16] Due to poor solubility in most organic solvents, all phenanthroline derivative ligands were not purified and were used directly to synthesize the iridium(III) complex salts. The synthetic procedure for the cationic iridium(III) complex salts contains two steps. The dinuclear cyclometalated iridium(III) chlorobridged precursor $[Ir(ppy)_2Cl]_2$ was synthesized by the same method as reported by Nonoyama.[17] Then the cationic iridium(III) complex salts were synthesized by the bridge-splitting reactions of $[Ir(ppy)_2Cl]_2$ and consequently coordinated with the corresponding phenanthroline derivatives. Compared with the synthesis of neutral iridium(III) complex containing β-diketone ligands, which needs harsh reaction conditions (reflux in a high-boiling solvent mixture) and much longer reaction time, the synthesis of cationic iridium complex salts $[Ir(ppy)_2(N\wedge N)]^+PF_6^-$ can be carried out under mild reaction conditions. In our case, new iridium(III) complex salts were obtained with lower decomposition, limited workup, and good yields. These complex salts were characterized by ^{1}H NMR, ^{13}C NMR, MALDI-TOF, and elemental analysis. However, the imidazolyl N−H signal in the N^N ligand of **1** could not be detected in d_6-DMSO solution from the ^{1}H NMR spectra.

Table 1. Crystallographic Data for 1

emipirical formula	$C_{43}H_{30}IrN_6Cl_4PF_6$
cryst syst	monoclinc
space group	*P*21/*c*
cryst size, mm	0.10 × 0.10 × 0.08
a, Å	14.079(3)
b, Å	12.862(3)
c, Å	23.706(5)
α, deg	90
β, deg	93.05(3)
γ, deg	90
V, Å^3	4286.7(15)
Z	4
calcd density, g cm^{-3}	1.719
μ, mm^{-1}	3.468
F(000)	2176
final R1 [$I > 2\sigma(I)$]	0.0396
wR2 [$I > 2\sigma(I)$]	0.0783
R1 (all data)	0.0779
wR2 (all data)	0.0901
GOF on F^2	0.964

Crystal Structure of 1. A single crystal of **1** was obtained from a mixed solution of CH_2Cl_2 and hexane. The ORTEP diagram of **1** is depicted in Figure 1. It can be seen that the iridium(III) center in **1** adopts a distorted octahedral coordination geometry. Selected relevant bond parameters of **1** and the previously reported iridium(III) complex $[Ir(ppy)_2(di\text{-}C_9H_{19}\text{-}bpy)]^+PF_6^-$ [11a] are listed in Table 2. All bond lengths and bond angles of **1** are within normal ranges.[11a] The metalated C atoms of the ppy ligands are in a mutually *cis* arrangement. The strong *trans* influence of the phenyl groups results in slightly longer Ir−N (N^N ligands) bond lengths than the distances of Ir−N (C^N ligands).[20] Similar to other related complex salts, the cation $[Ir(ppy)_2(N\wedge N)]^+$ is connected to the anion PF_6^- by weak intra- and intermolecular C−H---F−P hydrogen bonds with an average H---F distance of 2.56 Å and intramolecular N−H---F−P hydrogen bonds with an average H---F distance of 2.14 Å.

In addition, the molecular packing structure of **1** is shown in Figure 2. A significant degree of $\pi-\pi$ overlap with an interplanar separation of approximately 3.35 Å could be observed between the adjacent N^N ligands of **1**, which implies the existence of strong ligand (N^N)−ligand (N^N) ($\pi-\pi$) interactions.

Absorption Spectroscopy. The UV−vis absorption spectra of all complex salts are shown in Figure 3, and the electronic absorption data are listed in Table 3. For complex salts **1**, **2**, **4**, and **5**, intense absorption bands below 370 nm could be observed and are assigned to spin-allowed intraligand IL ($\pi \rightarrow \pi^*$) (ppy and phenanthroline derivatives) transitions. Moderately intense absorption bands in the range 370−440 nm and weak absorption

(18) Frisch, M. J.; Trucks, G. W.; Schlegel, H. B.; Scuseria, G. E.; Robb, M. A.; Cheeseman, J. R.; Montgomery, J. A., Jr.; Vreven, T.; Kudin, K. N.; Burant, J. C.; Millam, J. M.; Iyengar, S. S.; Tomasi, J.; Barone, V.; Mennucci, B.; Cossi, M.; Scalmani, G.; Rega, N.; Petersson, G. A.; Nakatsuji, H.; Hada, M.; Ehara, M.; Toyota, K.; Fukuda, R.; Hasegawa, J.; Ishida, M.; Nakajima, T.; Honda, Y.; Kitao, O.; Nakai, H.; Klene, M.; Li, X.; Knox, J. E.; Hratchian, H. P.; Cross, J. B.; Bakken, V.; Adamo, C.; Jaramillo, J.; Gomperts, R.; Stratmann, R. E.; Yazyev, O.; Austin, A. J.; Cammi, R.; Pomelli, C.; Ochterski, J. W.; Ayala, P. Y.; Morokuma, K.; Voth, G. A.; Salvador, P.; Dannenberg, J. J.; Zakrzewski, V. G.; Dapprich, S.; Daniels, A. D.; Strain, M. C.; Farkas, O.; Malick, D. K.; Rabuck, A. D.; Raghavachari, K.; Foresman, J. B.; Ortiz, J. V.; Cui, Q.; Baboul, A. G.; Clifford, S.; Cioslowski, J.; Stefanov, B. B.; Liu, G.; Liashenko, A.; Piskorz, P.; Komaromi, I.; Martin, R. L.; Fox, D. J.; Keith, T.; Al-Laham, M. A.; Peng, C. Y.; Nanayakkara, A.; Challacombe, M.; Gill, P. M. W.; Johnson, B.; Chen, W.; Wong, M. W.; Gonzalez, C.; Pople, J. A. *Gaussian 03, revision C.02*; Gaussian, Inc.: Wallingford, CT, 2004.

(19) Sheldrick, G. M. *SHELXTL-Plus V5.1 Software Reference Manual*; Bruker AXS Inc.: Madison, WI, 1997.

(20) Coe, B. J.; Glenwright, S. J. *Coord. Chem. Rev.* **2000**, *203*, 5−80.

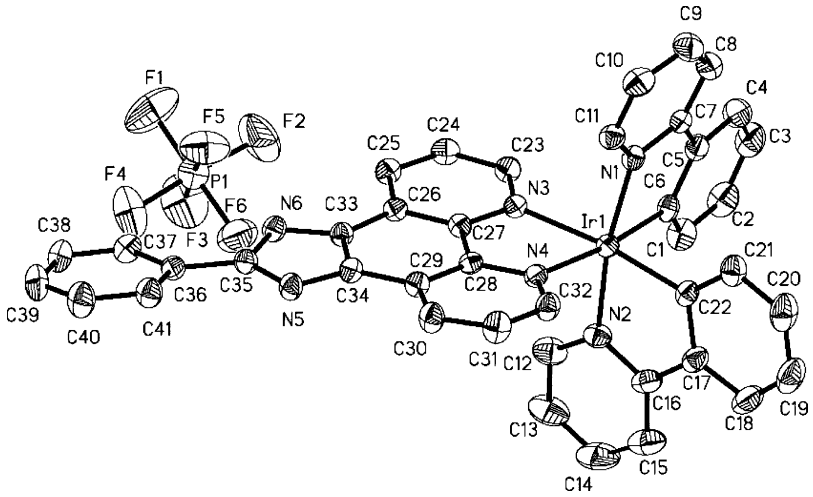

Figure 1. ORTEP diagram of **1** with the thermal ellipsoids drawn at the 30% probability level and the H atoms removed for clarity.

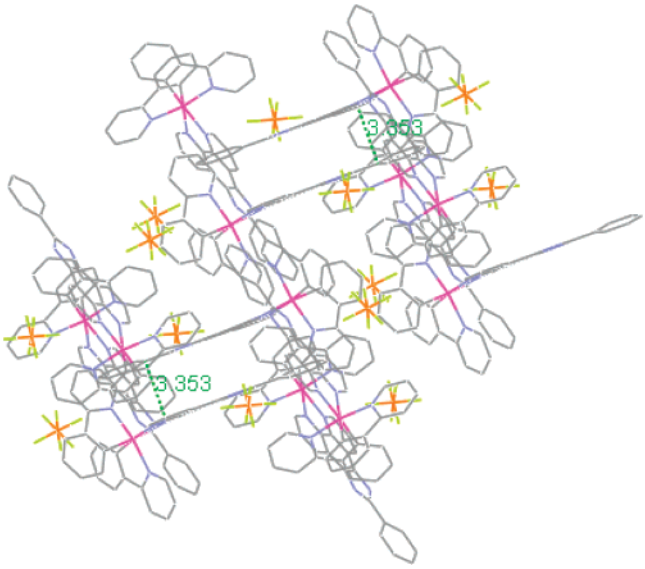

Figure 2. Molecular packing of **2** with the H atoms removed for clarity.

Table 2. Selected Bond Parameters (Å, deg) of 1

	1	[Ir(ppy)$_2$(di-C$_9$H$_{19}$-bpy)]$^+$PF$_6^-$ [11a]
Ir−C (Å)	2.009(5) 2.017(5)	2.015(7)
Ir−N$_{(CN)}$ (Å)	2.037(4) 2.042(4)	2.057(6)
Ir−N$_{(NN)}$ (Å)	2.139(4) 2.144(4)	2.151(6)
C−Ir−C (deg)	88.55(19)	94.5(4)
C−Ir−N$_{(CN)}$ (deg)	80.47(19) 80.7(2) 92.19(19) 93.34(19)	80.1(3) 94.9(3)
C−Ir−N$_{(NN)}$ (deg)	97.43(17) 97.21(17) 173.35(16) 172.76(18)	170.3(3)
N$_{(CN)}$−Ir−N$_{(CN)}$ (deg)	170.76(17)	172.7(4)
N$_{(CN)}$−Ir−N$_{(NN)}$ (deg)	96.32(16) 90.51(16) 93.10(15) 94.49(17)	89.9(2) 95.9(2)
N$_{(NN)}$−Ir−N$_{(NN)}$ (deg)	77.07(15)	76.3(3)

bands above 440 nm were also observed, which are assigned to spin-allowed metal-to-ligand charge-transfer ^{1}MLCT (dπ(Ir)→π*(phenanthroline derivatives and ppy)) transitions and

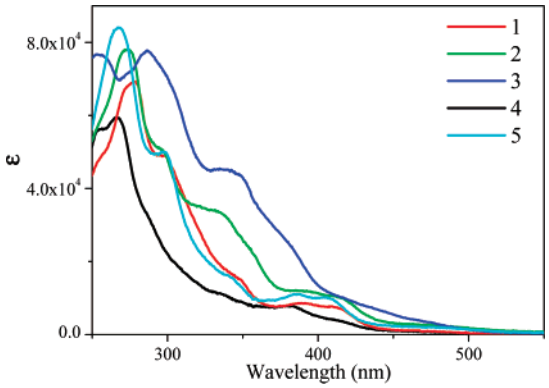

Figure 3. Absorption spectra of **1**−**5** in CH_2Cl_2 solution at a concentration of 1×10^{-5} mol L^{-1} at 298 K.

Table 3. Absorption Data of 1−5 in CH_2Cl_2 at 298 K

complex salt	λ_{abs}(log ϵ)/[nm]
1	279(4.84), 299(4.69), 348(4.18), 390(3.93), 416(3.85)
2	273(4.89), 296(4.71), 334(4.53), 393(4.07), 416(4.00)
3	286(4.89), 342(4.65), 379(4.41), 420(3.98)
4	266(4.78), 333(4.05), 383(3.90), 416(3.57)
5	267(4.92), 298(4.70), 341(4.20), 387(4.04), 410(3.98)

spin-forbidden ^{3}MLCT (dπ(Ir)→π*(phenanthroline derivatives)) transitions. For complex salt **3**, its ^{1}MLCT and ^{3}MLCT transitions are shifted to 400−460 nm and above 460 nm, respectively. The red shift and higher extinction coefficients (ϵ) of ^{1}MLCT and ^{3}MLCT transitions were observed when compared with those of other complex salts and ascribed to the presence of a carbazole fragment.

Luminescence Spectroscopy. The room-temperature photoluminescence spectra of all complex salts in CH_2Cl_2 solution and solid film are shown in the Supporting Information, and corresponding photoluminescence data of complex salts are summarized in Table 4. Figure 4 shows the photoluminescence spectra of complex salt **1** (as an example) in different conditions. It can be seen that all complex salts emit intense luminescence with similar emission wavelengths in the range 568−583 nm in CH_2Cl_2 solution at room temperature. The observed emission lifetimes in the microsecond and sub-microsecond time scales (Table 4) indicate the phosphorescent nature of the emissions. In addition, photoluminescence spectra of these complex salts in solid film were also measured and are similar to those in CH_2Cl_2 solution.

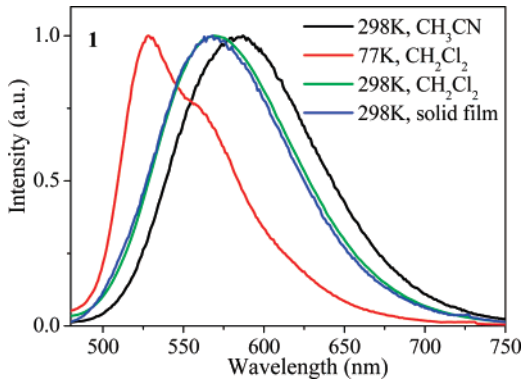

Figure 4. Photoluminescent spectra of **1** in different conditions. $\lambda_{ex} = 315$ nm.

Table 4. Photoluminescent Data of 1−5

complex salt	medium (T [K])	$\lambda_{PL,max}$ (nm)	Φ_{em}	τ (ns)
1	CH_2Cl_2 (298)	568	0.24	704.3
	CH_3CN (298)	587		
	solid film (298)	568		
	glass (77)	528		
2	CH_2Cl_2 (298)	583	0.22	469.0
	CH_3CN (298)	593		
	solid film (298)	584		
	glass (77)	528		
3	CH_2Cl_2 (298)	570	0.19	592.5
	CH_3CN	580		
	solid film (298)	577		
	glass (77)	529		
4	CH_2Cl_2 (298)	571	0.25	235.4
	CH_3CN (298)	583		
	solid film (298)	568		
	glass (77)	515		
5	CH_2Cl_2 (298)	572	0.22	538.2
	CH_3CN (298)	582		
	solid film (298)	580		
	glass (77)	524		

We also studied the low-temperature photoluminescence spectra of all complex salts in CH_2Cl_2 (Supporting Information). A blue shift of emission maxima was observed for all complex salts from fluid solution at room temperature to rigid matrix at 77 K, which was often observed for MLCT and LLCT emitters based on cyclometalated iridium(III) diimine complexes.[11] For typical MLCT emitters, such as the well-known $[Ru(bpy)_3]^{2+}$ complex and analogous compounds, such a blue shift is usually in the range 1000−2000 cm^{-1}, and it is also in the same range for Ir(III) cyclometalated compounds, which are reported to be pure MLCT emitters.[11c] Hence, for **1**−**5**, such slight blue shifts of <2000 cm^{-1} imply that the emissions of **1**−**5** are mainly assigned to MLCT transitions. The blue shift is caused by fast solvent reorganization in fluid solution at room temperature, which can stabilize the CT states before the emission takes place. However, at 77 K, this stabilization of CT states is hampered and the blue shift of emission maxima occurs.[11,21]

In addition, the photoluminescence spectra of all complex salts in different solvents were also investigated (see Supporting Information), and the data are summarized in Table 4. The emission maxima for all complex salts occur at higher energy in less polar CH_2Cl_2 than those in more polar CH_3CN, which is also very common for cyclometalated iridium(III) diimine MLCT emitters.[11]

Electrochemical Properties. The electrochemical properties of the complex salts were studied by cyclic voltammetry (see Supporting Information), and the data are listed in Table 5. An irreversible oxidation wave was observed at similar potentials between 1.03 and 1.10 V for all complex salts. It is assumed that pure metal-centered oxidation is reversible and irreversibility increases as the contribution to the HOMO of the cyclometalating phenyl(s) increases.[22] Therefore, the irreversible oxidation process is assigned to orbits receiving a strong contribution from the iridium center and Ir−C^- σ-bond orbits at the same time. Interestingly, an additional irreversible oxidation wave at 0.84 V was also observed for complex salt **3**. According to the previous report,[23] we assign it to the oxidation of carbazole. In addition, all complex salts exhibit a similar irreversible reduction wave at approximately −2.00 V. This reduction wave of **1**−**5** can be assigned to the reduction of the phenanthroline derivative ligands.

Table 5. Electrochemical Data for 1−5

	1	**2**	**3**	**4**	**5**
E^{ox}/V	1.03	1.05	0.84, 1.10	1.03	1.05
E^{re}/V	−1.98	−2.01	−2.01	−1.98	−2.01

Theoretical Calculations. To further investigate the nature of the excited state, density functional theory (DFT) for **1** and **4** was performed. The two complex salts have similar HOMO and LUMO distributions (Table 6). The HOMO distributions primarily reside on the iridium center and cyclometalated ligands. For **4**, the LUMO distribution is localized on the whole phenanthroline ligand (N^N ligand). Similarly, the LUMO distribution of **1** is only localized on the phenanthroline fragment. The imidazolyl group and the substituent phenyl group do not participate in the LUMO distribution. The calculated HOMO, LUMO, and energy of the triplet excited state (E_T) are listed in Table 6. The complex salts **1** and **4** show similar E_T values, which is in agreement with their similar electrochemical properties and emission wavelengths. Therefore, similar excited states and photophysical properties were observed for **1**−**5** with different imidazolyl groups and substituents on the imidazole.

Tuning Photophysical and Electrochemical Properties of 1−3 upon Addition of Anions. The complexation abilities of **1**−**3** with anions were investigated by UV−vis absorption titration experiments (Figure 5 and Supporting Information). For example, upon addition of F^-, the absorption bands of **1** at 277 and 404 nm gradually decrease and three new bands centered at 300, 338, and 476 nm start to develop with three distinct isosbestic points at 287, 385, and 415 nm (Figure 5), indicating strong ground state interactions between **1** and the fluoride anion, and a dramatic color change from weak yellow-green to brown can be observed with the naked eye (Figure 6). Similar phenomena were observed for complex salts **2** and **3** upon addition of the fluoride anion (Figure 5).

The emission spectra titration of **1**−**3** with anions was also measured. It can be seen from Figure 7 that the emission of the three complex salts is quenched upon addition of F^-. Moreover, similar changes in absorption and emission spectra of complex salts **1**−**3** were also observed when CH_3COO^- and $H_2PO_4^-$ were added (Supporting Information), which implied strong interaction between the complex salts **1**−**3** and these anions. However, no obvious spectral variations were measured for **1**−**3** upon addition of other anions (such as Cl^-, Br^-, I^-, NO_3^-, ClO_4^-, and CF_3COO^-). The binding constant values (K) for the three complex salts **1**−**3** calculated from fluorescence

(21) Juris, A.; Balzani, V.; Barigelletti, F.; Campagna, S.; Belser, P.; von Zelewsky, A. *Coord. Chem. Rev.* **1988**, *84*, 85−277.

(22) Calogero, G.; Giuffrida, G.; Serroni, S.; Ricevuto, V.; Campagna, S. *Inorg. Chem.* **1995**; *34*, 541−545.

(23) Stahl, R.; Lambert, C.; Kaiser, C.; Wortmann, R.; Jakober, R. *Chem.−Eur. J.* **2006**, *12*, 2358−2370.

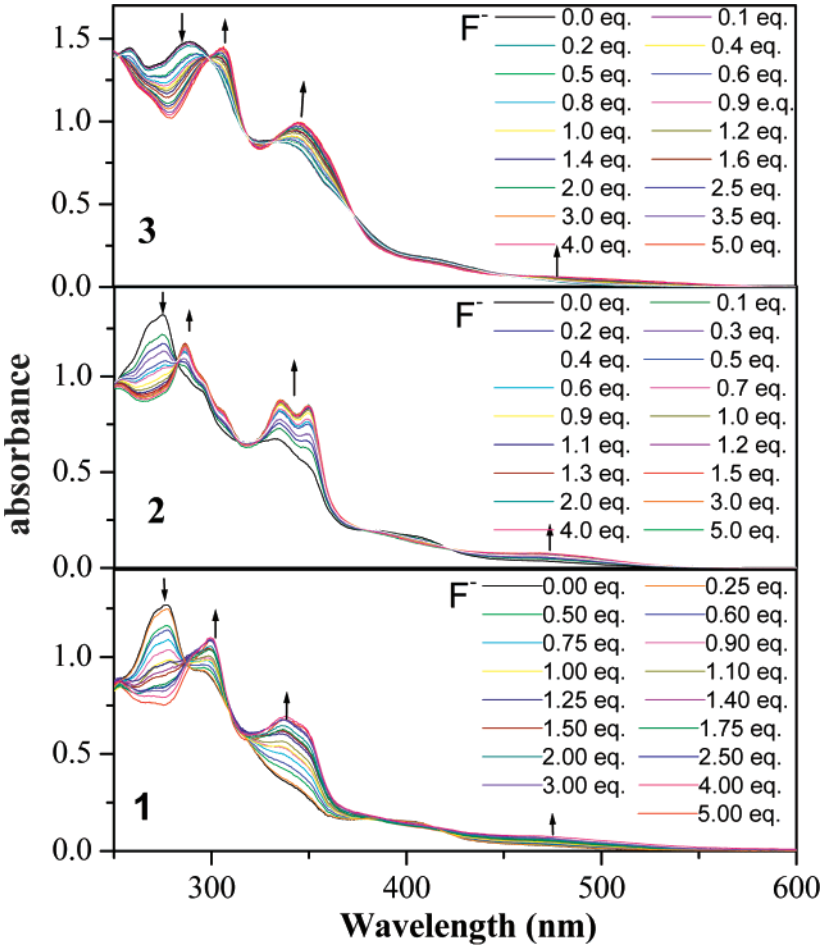

Figure 5. Changes in the UV−vis absorption spectra of **1**−**3** (20 μM) in CH_3CN solution with various amounts of F^-.

Table 6. HOMO and LUMO Distributions of 1, 4, and 1+H$^+$

Complex	HOMO	LUMO	E_{HOMO}(eV)	E_{LUMO}(eV)	E_T(eV)[a]
1	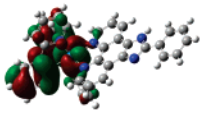	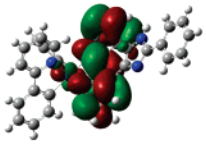	-7.71	-4.84	2.14
1+H$^+$	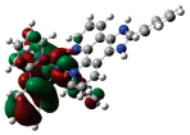	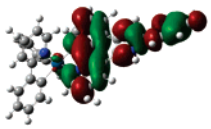	-9.71	-7.82	1.28
4	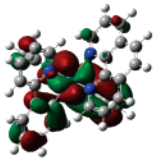	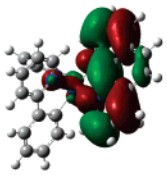	-8.01	-5.00	2.22

[a] Calculated energy levels of triplet excited state.

titration data are summarized in Table 7. We can see that the three complex salts **1**−**3** prefer to bind F^- and CH_3COO^- over $H_2PO_4^-$. Especially, the binding constant values (K) of **1** for F^-, CH_3COO^-, and $H_2PO_4^-$ were 7.01×10^4, 1.42×10^4, and 3.03×10^3 M^{-1}, respectively (Table 7). So, **1** can be used as a selective chemosensor for F^-.

To understand the optical response mechanism of **1**−**3** for anions, the response of **5** to F^- was also measured. No obvious change in UV−vis absorption and emission spectra could be observed for **5** upon addition of F^- (Supporting Information). Hence, we can conclude that the interaction of NH in the imidazolyl group of the N∧N ligand with anions is responsible for the significant optical variations. Unfortunately, we cannot demonstrate from the ^{1}H NMR titration experiments that the interaction of NH with anions is the formation of a hydrogen bond or deprotonation since the imidazolyl N−H signal could

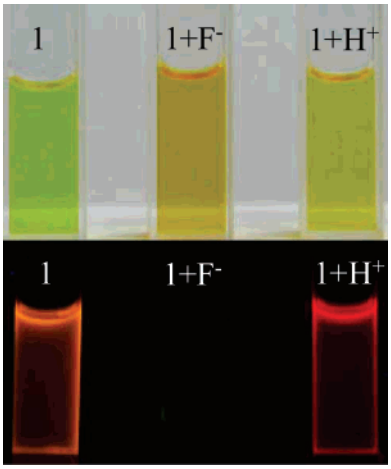

Figure 6. Color and emission color variations observed in acetonitrile solutions of **1** (5×10^{-4} M) in the presence of 2 equiv of F^- and CF_3COOH.

not be detected in d_6-DMSO solution from the ^1H NMR spectra. Recently, many anion sensors containing recognition moieties such as amide, urea, and thiourea with acidic protons have been reported to undergo anion-induced deprotonation.[24] In addition, the intramolecular N−H—F−P hydrogen bonds existing in these complex salts can also enhance the acidity of N−H, increasing the deprotonation trend.

Table 7. Binding Constants (K) of Complex Salts 1−3 for F^-, CH_3COO^-, and $H_2PO_4^-$ (M^{-1}) Determined from Fluorescence Titration Spectra

anion	1	2	3
F^-	7.01×10^4	9.62×10^4	3.86×10^4
CH_3COO^-	1.42×10^4	3.33×10^4	3.11×10^4
$H_2PO_4^-$	3.03×10^3	7.31×10^2	5.78×10^3

To better understand the optical response mechanism of **1**−**3** for anions, we measured the optical response of **1** to the weak organic base NEt_3 and strong bases Bu_4NOH (Figure 8). When strong bases such as Bu_4NOH were added into the solution of **1**, obvious spectral variations of the absorption and emission bands of **1** were observed, which are similar to those of **1** after addition of fluoride anion. In contrast, no obvious changes were observed upon addition of weak organic base NEt_3. This further confirms the suspicion that the reaction between the NH bond of the imidazolyl group of **1**−**3** and F^- is a deprotonation process and not a hydrogen-bonding effect.[25]

Furthermore, we also investigated the influence of fluoride anions on the electrochemical properties of **1**−**3**. After the addition of fluoride anions, no evident change was observed for the reduction wave (Figure 9 and Supporting Information), indicating that the interaction of anions with imidazole N−H does not change the LUMO energy level and distribution significantly. However, the addition of fluoride anions causes obvious variation of the oxidation wave (Figure 9 and Support-

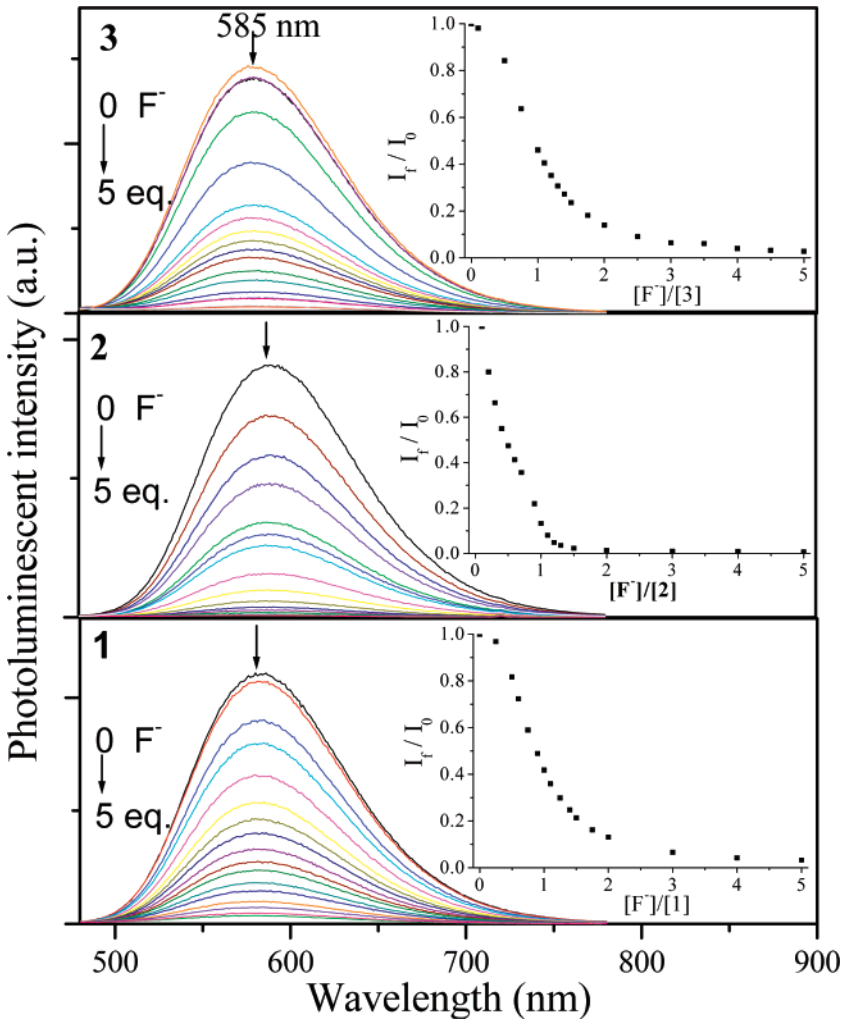

Figure 7. Changes in the luminescence spectra of **1**−**3** (20 μM) in air-equilibrated CH_3CN solution with various amounts of F^- ($\lambda_{ex} = 360$ nm). Inset: fluorimetric titration.

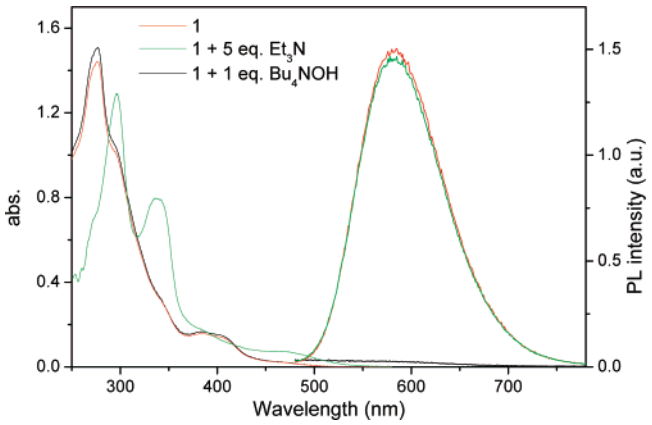

Figure 8. Response of UV−vis absorption spectra and luminescence spectra of **1** to Et_3N and Bu_4NOH.

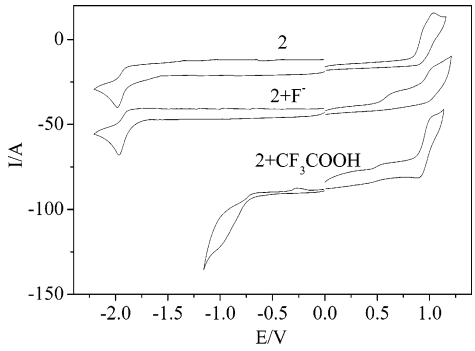

Figure 9. Cyclic voltammograms of **1** before and after addition of F^- and CF_3COOH.

ing Information). Upon addition of fluoride anions, the oxidation potential attributed to the iridium center and Ir−C^- σ-bond orbits was shifted positively, and a new irreversible oxidation wave appeared at more negative potential. The irreversible oxidation wave at 0.67 V could be assigned to the oxidation of the imidazolyl group after deprotonation.

The mechanism of fluorescence quenching in the presence of F^-, CH_3COO^-, and $H_2PO_4^-$ is somewhat ambiguous. Perhaps the deprotonation process results in a greater degree of distortion between its excited and ground state surfaces and increases the probability of radiationless transitions. In addition, there is also a probability of a photoinduced electron transfer (PET) process from the lone electron pair on the imidazolyl group after deprotonation, which quenches the emission of complex salts.

Tuning Photophysical and Electrochemical Properties of 1−3 upon Addition of CF_3COOH. Considering the imidazolyl group in the N^N ligands, sensitivity to protons might be expected for **1**−**3**. Herein, because of very weak interaction of

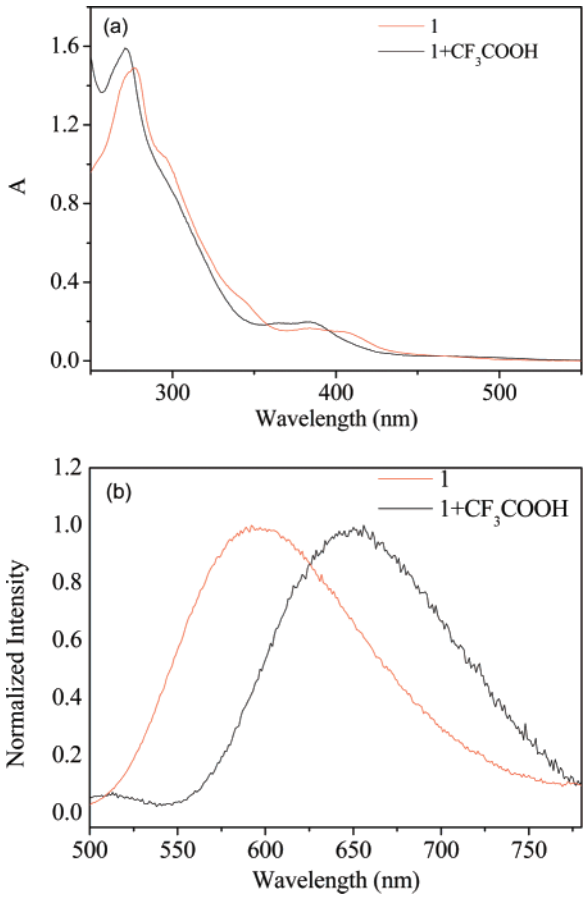

Figure 10. Absorption and photoluminescence spectra of **1** (20 μM) in CH_3CN solution before and after addition of CF_3COOH.

1−**3** with the anion CF_3COO^-, CF_3COOH was chosen as a source of protons. Significant changes in UV−vis absorption and emission spectra were observed when CF_3COOH was added into the CH_3CN solutions of **1**−**3** (Figure 10 and Supporting Information). For example, Figure 10 gives the variations of photophysical properties of **1** upon addition of CF_3COOH. In particular, upon addition of CF_3COOH, the emission wavelength of **1** was red-shifted and the emission color changed from yellow to red (Figure 6). Similar phenomena were observed for complex salts **2** and **3** upon addition of CF_3COOH (Supporting Information).

Because the addition of CF_3COO^- cannot induce the optical variations of the three complex salts **1**−**3** (Supporting Information), the evident changes in UV−vis absorption and emission spectra of **1**−**3** after the addition of CF_3COOH should be attributed to the interaction of a proton with **1**−**3**. To further understand this point, theoretical calculations on the adduct **1** + H^+ were performed, and the HOMO and LUMO distributions are shown in Table 6. Compared with **1**, no variation was observed for the HOMO distribution of **1**+H^+. However, there is a significant difference in LUMO distribution. The LUMO distribution of **1**+H^+ resides on the whole N^N ligand, whereas the LUMO distribution of **1** is localized only on the phenanthroline fragment of the N^N ligand (Table 6). In addition, the calculated energy levels of the HOMO and LUMO and the energy of the triplet excited state (E_T) for **1**+H^+ decrease markedly in comparison with those of **1** (Table 6), which is consistent with the obvious red shift of emission wavelength. So, protonation causes the imidazolyl and phenyl units to become involved in the LUMO, increasing the overall degree of delocalization and hence causing a large calculated stabiliza-

(24) (a) Cho, E. J.; Moon, J. W.; Ko, S. W.; Lee, J. Y.; Kim, S. K.; Yoon, J.; Nam, K. C. *J. Am. Chem. Soc.* **2003**, *125*, 12376−12377. (b) Gunnlaugsson, T.; Kruger, P. E.; Jensen, P.; Pfeffer, F. M.; Hussey, G. M. *Tetrahedron Lett.* **2003**, *44*, 8909−8913. (c) Lee, J. Y.; Cho, E. J.; Mukamel, S.; Nam, K. C. *J. Org. Chem.* **2004**, *69*, 943−950. (d) Vázquez, M.; Fabbrizzi, L.; Taglietti, A.; Pedrido, R. M.; González-Noya, A. M.; Bermejo, M. R. *Angew. Chem.* **2004**, *116*, 1996−1999; *Angew. Chem., Int. Ed.* **2004**, *43*, 1962−1965. (e) Boiocchi, M.; Boca, L. D.; Esteban-Gómez, D.; Fabbrizzi, L.; Licchelli, M.; Monzani, E. *J. Am. Chem. Soc.* **2004**, *126*, 16507−16514. (f) Amendola, V.; Boiocchi, M.; Fabbrizzi, L.; Palchetti, A. *Chem.−Eur. J.* **2005**, *11*, 120−127. (g) Boiocchi, M.; Boca, L. D.; Esteban-Gómez, D.; Fabbrizzi, L.; Licchelli, M.; Monzani, E. *Chem.−Eur. J.* **2005**, *11*, 3097−3104. (h) Gomez, D. E.; Fabbrizzi, L.; Licchelli, M.; Monzani, E. *Org. Biomol. Chem.* **2005**, *3*, 1495−1500. (i) Cho, E. J.; Ryu, B. J.; Lee, Y. J.; Nam, K. C. *Org. Lett.* **2005**, *7*, 2607−2609. (j) Esteban-Gómez, D.; Fabbrizzi, L.; Licchelli, M. *J. Org. Chem.* **2005**, *70*, 5717−5720.

(25) Liu, B.; Tian, H. *J. Mater. Chem.* **2005**, *15*, 2681−2686.

tion of this orbital, which is believed to be responsible for the obvious red shift of emission wavelength.

In addition, the electrochemical properties of **1**−**3** were also investigated upon addition of CF_3COOH (Figure 9 and Supporting Information). No evident variations of oxidation waves were observed for **1** and **2**. However, for complex salt **3**, the oxidation wave assigned to the carbazole fragment disappeared. This fact indicated that the carbazole fragment was also protonized after addition of CF_3COOH and the protonation made the oxidation of the carbazole fragment more difficult. Moreover, upon addition of CF_3COOH, the reduction waves of **1**−**3** assigned to the reduction of the N^N ligands were markedly shifted positively. So, protonation of the N^N ligand can reduce the energy levels of the LUMO more significantly and decrease the energy of the triplet excited state, which is consistent with the result of theoretical calculations.

Conclusions

In conclusion, we have synthesized a series of new cationic iridium(III) complex salts containing different imidazo[4,5-*f*]-[1,10]phenanthroline derivatives. The influences of anions and proton on the photophysical and electrochemical properties were studied in detail. After the addition of CF_3COOH, the emission wavelengths of the three complex salts **1**−**3** were significantly red-shifted and the emission colors changed from yellow to red. In addition, upon addition of F^-, CH_3COO^-, and $H_2PO_4^-$, the emission of the three complex salts **1**−**3** was quenched completely and the solution colors of **1**−**3** changed from yellow-green to brown, which can be observed with the naked eye. From the calculated binding constant values, we can see that **1**−**3** prefer to bind F^- and CH_3COO^- over $H_2PO_4^-$. Especially, **1** prefers to bind F^- over the other anions, suggesting that **1** can act as an ideal phosphorescent chemosensor for F^-. This preliminary understanding of the anion-sensing mechanism will actually help in the design of a series of new phosphorescent probes based on iridium(III) complexes by simply modifying the chemical structures of the ligands to contain a specific recognition site, which will also help in the exploration for new applications of iridium(III) complexes in chemosensors.

Acknowledgment. The authors acknowledge the financial support of National Natural Science Foundation of China (20490210 and 20501006), National High Technology Program of China (2006AA03Z318), and Shanghai Science and Technology Community (05DJ14004 and 06QH14002).

Supporting Information Available: Photoluminescent spectra and cyclic voltammograms of **1**−**5**, response of absorption and photoluminescence spectra upon titration with anions and CF_3COOH, and cyclic voltammograms of **2** and **3** before and after addition of F^- and CF_3COOH. This material is available free of charge via the Internet at http://pubs.acs.org.

OM700623J